ACS APPLIED MATERIALS & INTERFACES

Surfaces, Interfaces, and Applications

Fabrication of Hierarchical Micro/nano- Compound Eyes

Wenjun Wang, Jiang Li, Rongheng Li, Benqiang Li, Xuesong Mei, and Xuefeng Sun

ACS Appl. Mater. Interfaces, **Just Accepted Manuscript** • DOI: 10.1021/acsami.9b13355 • Publication Date (Web): 27 Aug 2019

is published by the American Chemical Society. 1155 Sixteenth Street N.W., Washington, DC 20036

Fabrication of Hierarchical Micro/nano- Compound Eyes

Wenjun Wang[1,2*], Jiang Li[1,2], Rongheng Li[3], BenQiang Li[3], Xuesong Mei[1,2], Xuefeng Sun[1,2]

[1] *State Key Laboratory for Manufacturing System Engineering, Xi'an Jiaotong University, Xi'an 710054, China*

[2] *Shaanxi Key Laboratory of Intelligent Robots, Xi'an Jiaotong University, Xi'an, 710049, China*

[3] *Department of Mechanical Engineering, University of Michigan, Dearborn, MI 48128, USA*

ABSTRACT: Fabrication of a hierarchical macro-/micro-/nano- compound eye is presented in this paper. This bioinspired compound (BIC) eye is obtained by an integrated manufacturing technology that combines (i) nano-imprinting, (ii) picosecond laser swelling, and (iii) air-assisted deformation. The diameter and height of nano-pillars, micro-lens and macrobase can be controlled precisely by fine-tuning the process parameters. The multifunctional properties of the BIC eye, such as superhydrophobicity, antireflection and other optical characteristics, are investigated. It is found that the micro-lens with nano-pillars can effectively improve the surface wettability with a contact angle (CA) of 152° and contact angle hysteresis of 12°, and enhance transmittance by 2% over the wavelength range of 200–1200 nm. Moreover, the final hierarchical compound eye exhibits the excellent imaging property and a wide field-of-view of 120° without distortion. These multifunctional properties will enable the widespread application of the compound eye in diverse real-time environmental conditions.

KEYWORDS: tertiary structures, bioinspired compound eye, surface wettability, antireflection, optical performance.

INTRODUCTION

In nature, a biological compound eye consists of a myriad of micron ommatidia arranged on a spherical macrobase and on the top of each ommatidia exist nanostructures.[1] This tertiary configuration endows the eye with a wealth of fascinating optical features such as a wide field of view (FOV), low aberration, high-sensitivity detection, and fast motion tracking.[2] For example, the nocturnal moth's eye called ommatidium is not only the basic imaging unit, but also serves as a key component connecting the on-top nanostructures and underneath millistructures. The on-top nanostructures could suppress the surface reflection and enhance photosensitivity in a dim environment; the curved distribution of ommatidium leads to the high FOV of a compound eye.[3-4] Due to its special configuration, the macro/micro/nano hierarchy inspired by the moth's eye are considered as ideal visual systems with multifunctional properties of miniaturization, multi-aperture, and large FOV, which may find applications in wide-view-angle imaging, fast motion detection, organic light-emitting diodes (OLEDs), solar energy devices, and other engineering systems.[5-7]

In the past decades, because of significant advantage over a single lens, artificial compound eyes have been studied by many groups and several fabrication strategies were proposed, including laser direct writing,[8-16] 3D configurations,[2, 17-19] or surface wrinkling.[20-21] These methods, however, do not render good control of the geometry and shape of lenslet due to their intrinsic limitations. Moreover, the stereo-type lens shape (round) and a larger size of ommatidia (400-1000 μm) of these artificial eyes

are much different from those natural ones, which would seriously degrade their optical performance such as resolution and signal-to-noise ratio.

Recently, researchers have developed more sophisticated hierarchical compound eye arrays. Wu et al. fabricated high-quality artificial macro-/micro- compound eyes, which provide high uniformity optics, constant resolution in all directions and distortion-free FOV from 30° to 90°.[22] Compound eyes of a 5 mm-diameter macrobase with 30,000 micro-size ommatidia were also reported,[23] which demonstrated the advanced imaging quality, the wide FOV and low aberration of the eyes. A compound eye with a high numerical aperture and anti-reflective nanostructures on curved surfaces was also made, and its optical property was studied.[24] More recently, Shao et al. fabricated micro-nano hierarchy and the water repellency property was studied. However, the secondary hierarchy cannot be used for optical purpose.[6] This is partly because the dopped material (Methyl red) degrade the imaging performance of the film. On the other hand, since the complex photothermal and photochemical reactions occur inside the material, the produced internal cavity causes several reflection of light. Raut et al. reported fabrication of micro-nano Arrays. The antireflection and antifogging properties were studied. Equally, the imaging performance was not studied due to material limitation.[25] Furthermore, the fabricated compound eye is also actually a micro-nano hierarchy. Compared with moth eyes with a milli/micro/nano hierarchical structure, the reported artificial compound eyes with a secondary configuration clearly have considerable limitations. For instance, with a macro/micro hierarchy, artificial compound eyes have a wealth of

micro-ommatidia on the macro-base but lack the nano-structures, thereby significantly limiting their capabilities in antireflection and self-cleaning.[8, 10, 22, 26-28] Moreover, for a micro/nano hierarchy, the field of view is greatly limited due to the planar distribution of microlens.[28-30] For an artificial eye to function as a natural compound eye, a micronanohierarchy (or a tertiary structure) needs to be integrated onto the macrobase. Despite the better performance potential of artificial compound eyes with a tertiary configuration, there appears to have been little, if any, on the subject. In essence, it so far has remained an elusive task to fabricate an artificial compound eye with a tertiary structure.

In this work, artificial compound eyes with a micronanohierarchy were fabricated by an integrated manufacturing technology of nano-imprinting, high-frequency picosecond laser swelling and air-assisted deformation. The well aligned nanostructures with controllable morphology and distribution on a large scale were made using the facile nano-imprinting technology; the direct laser writing was employed to create adjustable morphology; the curvature of spherical macrobase was controlled by an air-assisted deformation technology. The well-organized multiple steps allow preparation of artificial compound eye with tertiary configuration. Unlike the conventional method, not only an artificial compound eye with tertiary configuration was fabricated by proposed method, but also the hierarchy was transformed to optical material. Therefore, the artificial compound eye endows optical focusing, imaging, a large FOV with low aberration, wettability, and antireflection. The high optical performance of the artificial macro-/micro-/nano- compound eyes

was further verified through tests and measurements.

EXPERIMENTAL DETAILS

Preparation of materials

Polymethyl methacrylate (PMMA) doped with methyl red (MR) was selected as a swelling polymer, the matrix and the dye were both acquired from Aladdin Reagent Inc., China. PMMA and MR, with mass ratio of 1.5% were dissolved in toluene. After stirring with a magnetic stirring apparatus for 12 h, ultrasonic mixing for 40 min, the solution was filtered with a 200 nm filter paper to yield a solution of MR doped PMMA. The swelling polymer film was prepared on a glass plate by solution casting and solvent evaporation methods. After evaporating toluene at room temperature in a closed space for 6 h followed by post baking at 75° for 5 min, the doped-PMMA film with a smooth surface and uniform thickness was acquired. The thickness of swelling polymer here was controlled by adjusting the gap between the caster wall and the substrate in the casting process.

Fabrication of nanostructure

PMMA particles (20 g, available on Aladdin) were dissolved in Toluene (80 g) and magnetically stirred until completely dissolved, thus PMMA solution (mass fraction of 20%) was obtained. Subsequently, the porous alumina template and the slide were then cut into a 20*20 mm sheet, used as imprint template and substrate, respectively. And then PMMA solution of 150 mL was carefully squeezed out of a precision pipette, coated on the substrate, covered with petri dish and dried naturally

in a confined environment for 24 h. The obtained sample is completely adhered to the porous alumina with a dovetail clamp, put in an oven at 80℃ for 30 min. During the process, note that a glass with rubber film should be put between to guarantee a uniform contact. Finally, peeled off after cooling, the nanostructures were obtained. By controlling the applied time, nanastructures with different height can be obtained. Moreover, nanostructures with different morphology can be obtained by using different template. In the experiments, templates with diameter of 50, 70, 200, 300 nm were used.

Fabrication of microstructure

In the experiment, a green laser (532 nm wavelength) with a pulse duration of 10 ps and repetition rate of 10 kHz was used as the laser source. The optical system consists of a mirror, attenuator, diaphragm, shutter, lens (focus length of 25 mm) and motorized stage (movement accuracy of 50 nm). The continuously variable optical attenuator was used to control the energy delivered at the sample surface and the energy was measured by a power meter, which has a measuring range of 1 to 50 mW and a measurement accuracy of 0.001 nW. The electromenchanical shutter was used to controll the number of laser pulse irradiated on the sample. The motorized stage was used to achieve position control of the sample.

Fabrication of micro-/nano- structures

PDMS material and curing agent with a certain mass ratio (10:1) are widely used for pattern transfer process. In the experiments, the main and curing agent was first

fully mixed and placed in the vacuum oven to remove the bubble for 8 min. Pour the agent on the nanostructures, repeat the bubble removal process, and rest at room temperature for 12 h. The PDMS concave mold then was obtained. Subsequently, a drop of NOA-65 (UV curable expoxy resin, available on Taobao) was dropped on the as prepared dopped-PMMA sample (obtained through the material preparation process), put the PDMS concave mold on it, UV exposure to fully cure, peel off and the sample for laser swelling was obtained. The addition of NOA-65 film could not only support the notop nanostructures but also prevent gas leakage produced through laser-matter interaction and thus guarantee the height of micro-/nano- structures. The micro-/nano- structures finally were obtained by laser rear-side modification. The optical set up was mentioned above. Through adjusting the laser power and irradiation time, the morphology of microstructures could be controlled.

Fabrication of multiscale artificial compound eyes

Again, another replication was used for pattern transfer process. The 184 compounds with the mass ratio of the main and curing agent (10:1) were used. Equally, the vacuum oven was used to remove the bubble. Then, the 184 compounds were prepared on the micro-/nano- structures using the spin coating method, with a speed of 500 rpm for 18 s. Subsequently, the whole material was placed in the oven at 80 ℃ for 1h, released, and fixed on a homebuilt mold and negative air pressure ranging from 0.7 MPa to 1 MPa was applied; the height of macrobase was adjusted easily by controlling the film thickness and air pressure. The dependences of base height of fabricated microbase on film thickness and applied negative pressure are

shown in Figure S1. After the pressure was stable, the NOA-65 was poured into the deformed polymer cavity, covered with coverslip (20 mm × 20 mm) and fully crosslinked for 5 min with UV light. Peeling off, the multiscale compound eye was obtained.

Measurement and characterization

The structures were characterized using a scanning electron microscope (HITACHI). The morphology of microstructures was analyzed using a laser scanning confocal microscopy (Olympus OLS4000, Japan). The CAs of water droplet on hierarchical surfaces was measured using an optical contact angle measuring and contour analysis systems (OCA 20 system, Dataphysics, Germany), which combine high resolution optics, exact liquid dosing and precise sample positioning into powerful and reliable measuring systems. The CA of each sample is the average of measurements at five different locations. The experiment was conducted at ambient temperature. Before the measurement, a layer of fluorocarbon was deposited with C_4F_8 using a Plus 100 system (Oxford Instruments, UK). Reference water droplets of 5 μL were used for CA measurements. The surface reflectance of samples was measured using a spectrophotometer (Shimadzu UV3600).

RESULTS AND DISCUSSION

Figure 1 schematically illustrates the fabrication procedure used to create biomimetic hierarchical macro-/micro-/nano- compound eyes. Firstly, two polymer films were prepared on a glass substrate for nanoimprinting and laser swelling,

respectively. After preparation of polymer films, the nano-structure of the hierarchical surface is created by nano-imprinting, as shown in Figure 1a. A PDMS soft mold replicated from a structured silicon wafer was used to ensure uniform contact between the substrate and the mold using the pattern transferring process. Then, the micro-structures are created using the laser swelling method, as shown in Figure 1b. Because of the careful selection of materials and laser sources, deviation in nano-structure was negligible and fully-covering hierarchical structures are formed. For reconfigurable microtemplating, a homebuilt mold with a 5-mm diameter circular chamber was attached to the vacuum pump. An annular groove was designed to fix the membrane. The macro-structures were obtained using air-assisted technology, as shown in Figure 1d. After the second PDMS molding and the photosensitive polymer resin (SU8) molding, the fully covering hierarchically macro-/micro-/nano-compound eyes were formed, as shown in Figure 1g. Figure 1h shows the optical system used for the swelling process. The picosecond laser successively passes through mirror, attenuator, diaphragm, shutter, lens and finally focused on the as-prepared sample.

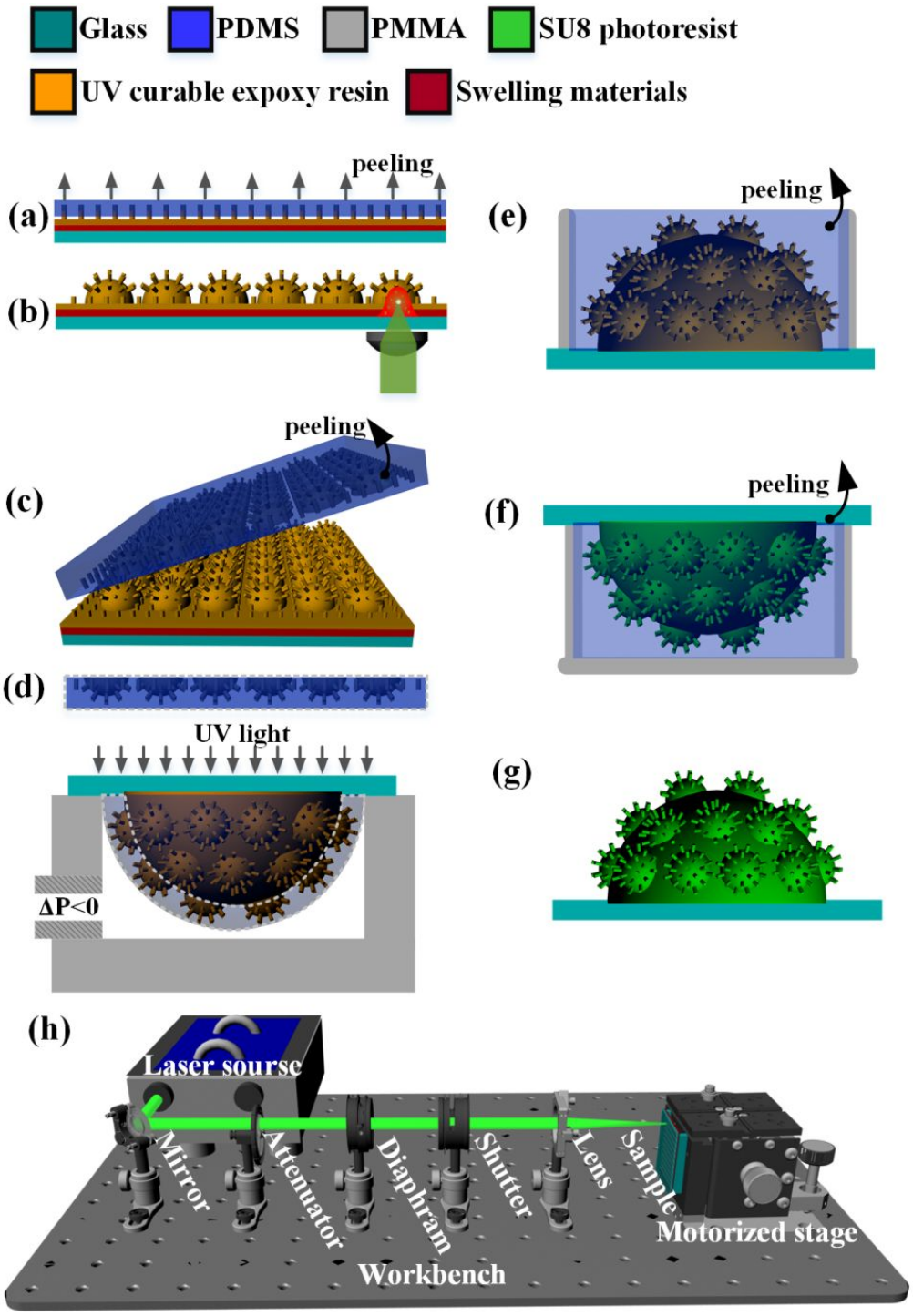

Figure 1. Schematic diagram of the fabrication process. (a) Pillar arrays are fabricated using nano-imprinting technology. (b) Laser beam is irradiated on the swelling layer to form micro-structures from the side of substrate. (c) A reconfigurable microtemplating process and micro-nano template was obtained. (d) Replication with UV curable expoxy resin. Dotted line

shows distribution transition of MLAs. (e) Second PDMS molding. (f) Photosensitive polymer resin (SU8) molding. (g) Formation of hierarchically macro-/micro-/nano- structure. (h) Optical system used for the swelling process.

Fabrication and Performance of Nano-structures

Nanoimprinting is a promising nanostructure manufacturing technology with the advantage of making nanostructures over a large area with high efficiency. As part of tertiary structure of the compound eyes, nanostructure should have a smaller size than light wavelength to enhance the light absorption and hydrophobicity of lens. For this purpose, porous alumina is adopted as the mold of nanoimprinting in this study, because it has the unique geometry and diverse nano-size hole-structures. Due to the high deep-to-width ratio of porous alumina mold, nano-pillar arrays will become clusters after the mold is completely filled. To overcome this problem, we adopted the incomplete filling method to obtain nano-structures.

Morphology of the Fabricated Nanopillars

The morphology of nanopillars fabricated in different imprinting times of 10-60 min were obtained (as is shown in Figure 2a, the imprinting temperature was 80 ℃). As the imprinting time is 10 min, only hexagonal cell superficial structures are obtained; when the imprinting time increases to 20 min, the nano-pillar structures are produced, but they are too short in height; when the imprinting time continues to 40 min, the regular and ordered nano-pillars with enough height are produced. With too long an imprinting time, say, of 60 min, the nano-pillars become clustered. Generally,

with an increase in imprint time, growth in height of nanostructures with good uniformity can be obtained. However, when the imprint time reaches 60 min, the nanopillars become clusters, which may result in deterioration of water repellency and antireflection performance. This was verified in the later characterization of fabricated structures. Thus, care needs to be exercised to control the imprinting time in order to achieve high-quality nano-pillar arrays.

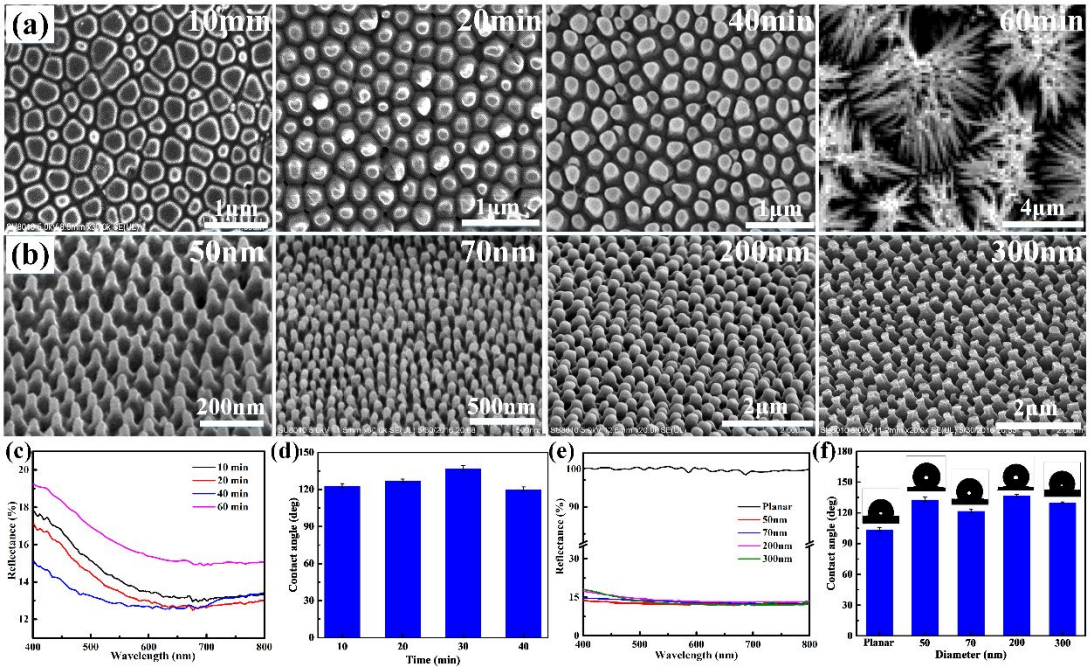

Figure 2. Morphology and characterization of nanostructures. (a) SEM images of nanostructures fabricated with imprint time of 10-60min. The imprint temperature was 80 ℃. The diameter was the same of 200 nm. (b) SEM images of nanostructures with different diameter were fabricated. The imprint time was 30 min. (c,f) Characterization of fabricated structures. (c,d) and (e,f) are contact angle and surface reflectance of structures with different height and diameter.

Surface Reflection and Wettability of the Nanopillars

The optical property and wettability of nano-structures imprinted in different

times are shown in Figures 2c and 2d. With an increase in imprint time, the light reflectance of nano-structures drops continuously. The nano-pillars imprinted for 40 min have the optimal light absorption due to their enough height and regular shape. It is noteworthy that the cluster structures over-imprinted for 60 min have the worst light absorption. The imprinting time and the morphology of nano-structures have the similar effect on wettability, as shown in Figure 2d. The surface with nano-pillars imprinted for 40 min has the largest contact angle about 135°, while the nano-clusters imprinted for 60 min has the lowest contact angle.

With an optimal imprinting time, nano-pillars with different diameters from 50 nm to 300 nm are fabricated, as shown in Figure 2b. Compared with a planar surface, nano-pillars decrease the light reflectance to a large extent, as shown in Figure 2e. Meantime, the wettability is also improved remarkably under the action of nano-pillars, as shown in Figure 2f. In contrast to the height and shape, the diameter of nano-pillars has little effect on optical property and wettability. In whole, nano-pillar structures with the excellent optical property and wettability are fabricated, which can meet the functional need of the tertiary structure of hierarchically compound eyes.

Mechanism for the Antireflective and Hydrophobic Effect of the Nanopillars

Geometrical structure is very important for wettability of artificial compound structures. To fabricate nanostructures with better performance, it is needed to understand the relationship between nanostructures and its hydrophobic behavior. At

present, Wenzel model and Cassie–Baxter model are basic guidelines for study of hydrophobic surface. Due to the hydrophobic state of droplet in the experiment, Cassie–Baxter model is favorable. The wettability on a nanostructured surface can be described by the Cassie-baxter theory. This theory can be described as follows:[12, 28-29]

$$\cos\theta = r_f \cos\theta_Y + f - 1 \quad (1)$$

where θ is the Cassie–Baxter CA, θ_Y is the Yong CA for an ideal surface, f is the fraction of solid surface wet by the liquid, and r_f is the ratio between the actual and projected solid surface area. According to the theory, the gaps between nanopillars could prevent a complete contact of liquid with the solid surface, thereby giving to an improved surface hydrophobic effect. This explains why hydrophobic performance is better with an introduction of nanopillar arrays on the planar surface. With an increase in height of nanostructures, the surface becomes rougher and the air-trapping ability improves, and thus a larger CA was observed. However, when imprint time was set at 60 min, the nanoclusters formed reduce the air-trapping, thereby deteriorating the hydrophobic performance.

Traditionally, there are two approaches adopted to suppress the Fresnel reflection: addition of multiple layers with various RI values and introduction of nanostructures at the interface of air and substrate, like a moth eye. The idea is to reduce the discontinuity of the refractive index at the interface, and thus to produce a gradual index gradient. According to the effective medium theory, the effective refractive index of inserted layer can be calculated as follows:[26-27]

$$n_{eff} = \sqrt{n_1^2 f + n_2^2(1-f)} \quad (2)$$

where $n_1$and n_2 are the refractive index of air and the substrate, respectively. Also f is the fill factor of antireflective nanostructures. In the study, the addition of nanopillars on planar surface as an inserted layer provides a stepped refractive index variation. Therefore, a lower surface reflectivity is expected. With imprint time increased (for the times of 10-40 min), the height of nanostructures increases, providing a more gradual index gradient. As a result, a lower surface reflection was found with an increased imprint time. With the imprint time of 60 min, the over-imprinted clusters decrease the effective height of nanostructures, reducing the effect of index variation at the substrate/air interface. This results in deterioration of the anti-reflection performance and therefore, a large surface reflectivity was found.

It is found, however, that the variation in nanopillar diameter has little effect on surface reflective and hydrophobic effect. This is because a longer imprinting time generates a higher pillar, leading to a significant increase in aspect ratio. This improves both the air-trapping and light-trapping abilities of nanopillars. However, for the same height, an increase in diameter would not generate a significant variation in aspect ratio. Conseuqently, the height of nanopillars has a great influence on surface reflection, while the effect of diameter variation is practically negligible.

Experiments showed that the height of nanopillar is the dominant factor that affects antireflection and repellency property. By controlling the imprint time, the height and aspect ratio of nanopillars can be adjusted by the cost effective and simple

technique to control water repellency and antireflection. The advantages of this method lie in its ability to replicate high aspect ratio structures and meantime provides potential for the large area macro-nano compound structures.

Fabrication and performance of hierarchically micro-/nano- compound eyes

Mechanism and Fabrication of Microstructues by Laser Swelling Technology

In this paper, picosecond laser swelling is used to fabricate the secondary structure of hierarchically compound eyes, which is also called ommatidia. In contrast to other fabricating methods for ommatidia, ultrafast laser swelling has the remarkable advantages of controllable shape, size and distribution of micro-lens. In particular, with the same lens aperture, the height of micro-lens can be improved substantially and thus the FOV of micro-lens can be increased by means of laser swelling.

The formation of a swelled structure is attributed to both photochemical reaction and thermal softening.[32-34] Upon irradiation on the dopped-PMMA film, two molecular processes occurs simultaneously.[6, 13, 32-35] This leads to photolysis of the dye and molecular relaxation, which triggered the generation of small gaseous products and heating of the matrix. Because the volume of produced gas product is much larger than that the original MR molecules, free-volume increases inside interlayer and the subsequent volume relaxation is responsible for production of final swelling.[35] Meanwhile, the transient high temperatures on the surface of sample induced by laser irradiation also increase the temperature-dependent internal pressure and soften the matrix polymer, which contributes to the volume increase of doped

PMMA. Due to the different absorption, PMMA and Methyl-red molecular exhibit different characteristics. Figure 3a and 3b show the molecular formula of the adopted swelling polymers, and the absorption spectra of MR-doped PMMA and pure PMMA, respectively. It can be seen that the polymer is more active to the photons with wavelength range of 200-300nm, while the dye molecular has a different absorption range of 400-600 nm. This means the decomposition of PMMA doesn't occur upon green light irradiation. The photolysis of dye molecular leads to the formation of the final products and the release of heat. The generation of gaseous product and softening polymer both guaranteed the swelling formation:[32-33]

$$C_{15}H_{15}N_3O_2 \rightarrow CO + CO_2 + NO + NO_2 + H_2O \quad (3)$$

Laser power and irradiation time are two key parameters to control the size and shape of micro-lens by laser swelling. With a fixed irradiation time of 0.5 s, the dependence of the diameter and height of micro-lens on the laser power is shown in Figure 3a. With the increase of laser power, the diameter and the height both enlarge obviously. When the laser power increases to some extent, the diameter of micro-lens is nearly constant, while the height of micro-lens continues to ascend. With a laser power of 19 mW, the diameter and the height of micro-lens are 94 μm and 37 μm, respectively.

The fidelity of large-area micro-lens array is closely related to the optical property of compound eyes. In order to obtain the micro-lens array with high consistency, the laser power should be stable with a minimum fluctuation in the

fabricating process. So, the laser power of 10mW is selected as an optimal parameter to determine the relationship between the size of micro-lens and the irradiation time, and the results are given in Figure 3b. With laser irradiation time increased, the diameter of micro-lens increases slowly until it reaches a saturation, whereas the height increases sharply. With the irradiation time of 4 s, each micro-lens is about 93 μm in diameter, and about 61 μm tall. If the irradiation time is let continue to increase, the upper surface of micro-lens will be broken. In sum, the diameter and height of micro-lens could be tuned by varying the laser power and irradiation time; consequently, the micro-lens with large-range FOV and longer focal length are achieved.

Figure 3 also shows the laser scanning confocal microscope (LSCM) observations of the micro-lens array. The tuned diameter and height of the micro-lens are close to the ommatidia of natural compound eyes, which have strong potential in compound eye inspired optical devices. Highly uniform, no shape distortions can be found in the LSCM images, indicating the capability of the present method for fabrication of high-quality micro-lens.

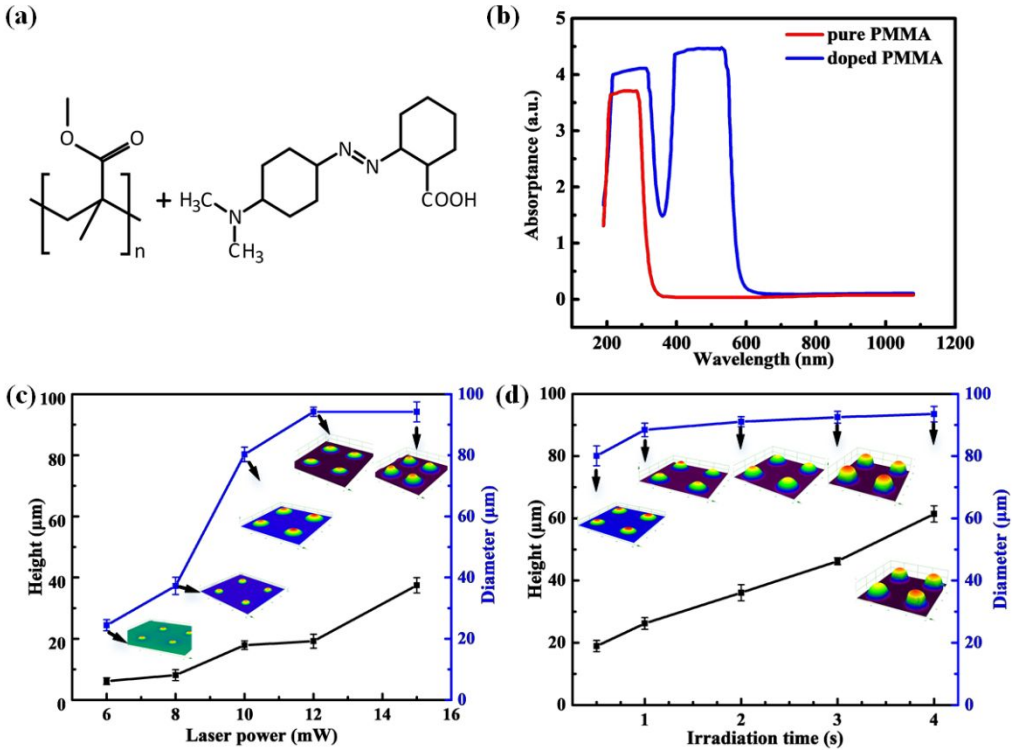

Figure 3. (a) Molecular formula of the adopted swelling polymers, MR and PMMA. (b) Absorption spectra of MR-doped PMMA and pure PMMA. The dependences of the diameter and height on the laser power (c) and irradiation time (d), respectively. The black arrow shows the laser scanning confocal microscope of fabricated structures. The irradiation time for (a) was 0.5 s, and the laser power for (b) was 10 mW.

Fabrication and Morphology of Micronano Compound Structues

As discussed above, micro-/nano- compound structures are fabricated by means of laser swelling and nano-imprinting. Methyl red (MR) doped Polymethyl methacrylate (PMMA) and UV- curable prepolymer were chosen as the swelling polymer and imprint polymer, respectively. According to the absorption spectrums, two polymers have a different absorption characteristic over a wavelength range which is higher than ultraviolet band and smaller than 550 nm. Therefore, the

micro-lens here is fabricated with a 532 nm picosecond laser. A high absorption of the underlying swelling polymer can ensure the essential volume increase, while a low absorption of the superposed imprint polymer can avoid the damage of pre-formed nano-pillars.

To integrate the nanostructures on the micro-lens, a layer of polymer was introduced. Besides supporting the on-top nanostructures for imprinting to follow, the prepared upper layer also prevents the burst of microstructures during the subsequent swelling process. However, the addition of the confined layer affects the laser-matter interaction and thus a different size variation is expected. Therefore, the dependence of micro-lens on laser power with confined layer should be further evaluated.

Figure 4a shows the dependence of height and diameter of micro-lens on laser power with the confined layer. The diameter and height of micro-structure first increase with laser power increasing until 10mW. Then the size of micro-lens slightly decreases and reaches a stable state at a power range of 12-20 mW. Over this range, the size of micro-structures remained almost unchanged with laser power. Generally, the laser-matter interaction can be divided into two stages: size rise and stable period. At the first stage, with more energy irradiation on the material, more gaseous product was emitted. Meanwhile, the upper confined NOA-65 layer could prevent the gas leakage and the produced internal stress contributes to the increase in micro-lens size. However, with more energy irradiated on the material, the restraining force results from deformation of the upper layer material would limits the further expanding of the confined gas product and therefore the size of micro-structure becomes saturated.

In the experiment, the diameter and height of micro-lens could be controlled in the range of 5-57 μm and 5-28 μm, respectively.

The SEM characterization of micro-/nano- hierarchically compound ommatidia with different height of micro-lens is shown in Figures 4b and 4c. Because the nano-structures are fabricated prior to micro-lens, the deformation of nano-structures is inevitable after the micro-lens is formed. When the curvature of a micro-lens is small, the nano-structures have a relatively uniform distribution around the positions of P1 and P2, as shown in the insets of Figure 4b. With the increase of the curvature of micro-lens, the ontop nanostructures are somewhat damaged and the period of nanostructures becomes inhomogeneous for the position of P3, as shown in the insets of Figure 4c. Obviously, at the top of micro-lens, nanostructures have a much larger deformation than that at the bottom.

Surface Reflection and Wettability of Micronano Compound Structures

In order to study the effect of compound structures on the performance of antireflection and wettability, the contact angles and light absorption of micro-/nano-compound structures are measured and compared with planar without surface structures. The results are given in Figure 4d. Compared with the simple nano-structures (shown in Figure 2f), the wettability of micro-/nano- structures is further improved and the contact angle reaches 152°. Furthermore, the forward and backward sliding angles were measured to be 142° and 154°, respectively, as shown in inset in Figure 4d. Thus, the contact angle hysteresis, which was defined as the

difference between forward and backward sliding angle, was 12°. This is the result of the combined action of micro-lens and nano-pillars. The high static contact angle and low contact angle hysteresis indicates high mobility of droplet on the fabricated textured surface, which shows potential for self-cleaning applications. As regards to optical property, the micro-/nano- structures decrease the light reflectance of polymer material surface from 100% to about 22% within the wavelength 400-800 nm, and thus exhibit an excellent capability of antireflection. Compared with other reported work (<10%),[4, 25, 31] the reflection by the fabricated hierarchy is relatively high. This is because the sparse distribution and smaller height of fabricated nanopillars. In addition, the light absorption of micro-/nano- compound structures, however, is somewhat less than that with nano-structures (shown in Figure 2e). This may be attributed to the deformation of nano-pillars in the formation process of micro-lens. From a different perspective, this phenomenon confirms that the nano-structures are the dominant factor in determining the light absorption of the hierarchically compound eyes and thus they are indispensable in the high-quality artificial compound eyes. In the further study, the deformation of nano-pillars needs to be corrected through some process like pre-compensation of the height and density of nano-pillars before the fabrication of micro-lens.

Mechanism for Antireflection and Hydrophobicity of the Micronano compound structures

By the effective medium theory, the antireflection of nanostructured surface is considered as an inserted layer for stepped refractive index. For nanostructured and

hierarchically structured surfaces, the much lower surface reflectivity was found. In theory, the hierarchical structures have an effective antireflection capability by providing a more gradual refractive gradient. However, in the experiment, the on-top nanopillars experience deformation during the swelling process, and thus the antireflection performance deteriorates compared with the nanostructured surface.

For a rough surface, the liquid may not complete penetrate inside the cavities, leading to a formation of air pockets. According to the Cassie-Baxter theory, surface roughness and the fraction of solid surface wet by the liquid are main factors that affect the surface wettability. Furthermore, it can be deduced that an increase in roughness results in an increase in Cassie–Baxter CA, whereas f is negatively correlated with the CA. In the experiment, the roughness of nanostructured and the hierarchical structured surfaces is higher than that of planar surface. As a result, the largest contact area between the droplet and the surface is found on a flat surface, but is reduced on a nanostructured surface and yet minimized on a hierarchical structured surface. This is why the contact angle of flat surface is smallest (~108 °) and the hierarchical compound surface is the largest (~152°).

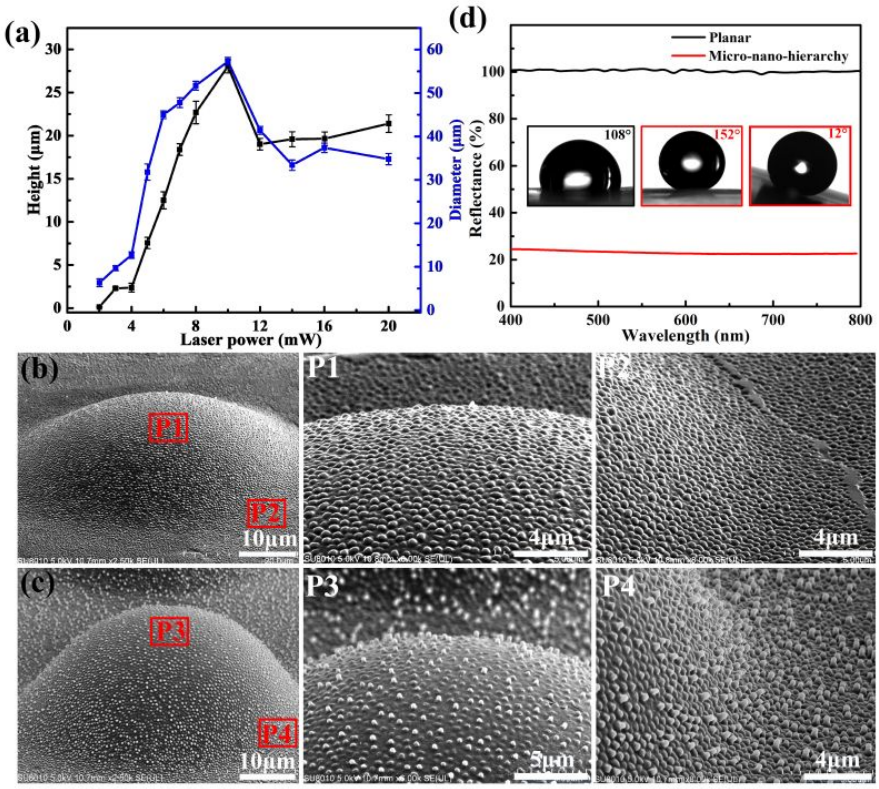

Figure 4. (a) Dependence of morphology of microstructures on laser power with confined layer. The irradiation was 2 s. (b,c) Micro-/nano- compound structures with different height of microstructures. (b) Micro-/nano- compound structures with small curvature. P1 and P2 are partial magnification of two different positions. (c) Micro-/nano- compound structures with high curvature. P3 and P4 are partial magnification of two different positions. Characterization of micro-/nano- compound structures. (d) Reflectance of hierarchy and planar surface. The insets are contact angles on the planar and hierarchical surfaces.

Fabrication and performance of hierarchically macro-/micro-/nano-compound eye

The bioinspired compound (BIC) eye with a macro-/micro-/nano- hierarchical structure was fabricated (see Figure 5a). The diameter and height of the macrobase

can be adjusted precisely by the change of mold size and air pressure. The micro-ommatidia are uniformly distributed on the macrobase, on which dense nano-pillars clearly assume an orderly arrangement.

Imaging and Weak Light Detection of Fabricated Compound Eye

In order to characterize the optical property of this BIC eye, a system comprising a 3D positioning stage, an objective lens, a tungsten lamp and a CCD camera was set up. In the measurement, a mask with the letter "A" was placed between the light source and the hierarchically compound eye. The BIC eye exhibits high optical uniformity and imaging functions. As shown in Figure 5b, the equivalent and clear imaging of the letter "A" was observed. Owing to the nonplanar distribution of the microlens, the focal points of each unit are not in the same horizontal plane. It is noted that every unit of the BIC eye can form a sharp image, and the images exhibit a high optical uniformity owing to the high quality and uniformity of the ommatidia, which ensures the application of the BIC eye in micro-imaging and sensing systems. Meantime, the effect of the BIC eye on the suppression of reflectance is evaluated through the measurement of the transmittance of the samples. The optical characterization system is set up, as shown in Figure 5c. The characterization system consists of a laser source with a wavelength of 475 nm, a diaphragm, an attenuator, and a power meter. The diaphragm was used to shape the beam. The continuous attenuator was used to adjust the laser power. The laser beam was directed at the interface of the bottom of lens and photodetector at a total reflection angle. A power meter was used to measure the laser power transmitted through the sample.

The transparency is of great importance in various applications, such as solar energy devices, image sensors and artificial compound eye. Figure 5d shows the transmittance comparison of compound eye with a tertiary configuration of macro-/micro-/nano- structure and an ordinary eye. Apparently, with the increase of incident laser power, though the laser power transmitted through the sample increases for both the BIC and ordinary eyes, the former has a significantly higher transmittance power that the latter. This means that the ommatidia with nano-pillars could effectively suppress the reflectance of the incident light. Furthermore, with the increase of incident power, the relative transmittance power of the BIC eye gradually decreases and finally stabilizes, which suggests that the BIC eye has better anti-reflection performance, especially for weak light. In whole, the BIC eye with a hierarchical macro-/micro-/nano- structure has an excellent light transmittance and weak light detection capability.

In the present work, the transmittances of surfaces with and without micronano hierarchy were measured in the wavelength range of 200-1200 nm. As shown in Figure 5e, the transmittance of micro-nano hierarchy is slightly higher than that without micronano hierarchy and the rising ratio is ~2%. Compared with the high antireflection and superhydrophobicity performance by addition of nanostructures on the microlens, the existence of nanostructures affects the transmittance to a small extent. From the experimental result, it can be seen that the transmittance is ~78% and remains stable in the visible spectrum. For wavelength larger than 800 nm, the transmittance vibrates violently but still have high transmittance (>70%); whereas the

transmittance decreases dramatically to ~1% with wavelength smaller than 300 nm. Peng et al. reported that the improved transmittance of substrate was observed by addition of well-aligned nanostructures (the transmittance is ~90%), which is higher than that in our work (~78%),[4] while the water repellency performance is worse (~130°) than that in our work. The work by Ahsan et al. showed that the transmittance deteriorates for laser ablated surface (~80%). This is because that the random distribution of irregular nanostructures influences the light transmission and the transmittance becomes unstable in the visible range.[36]

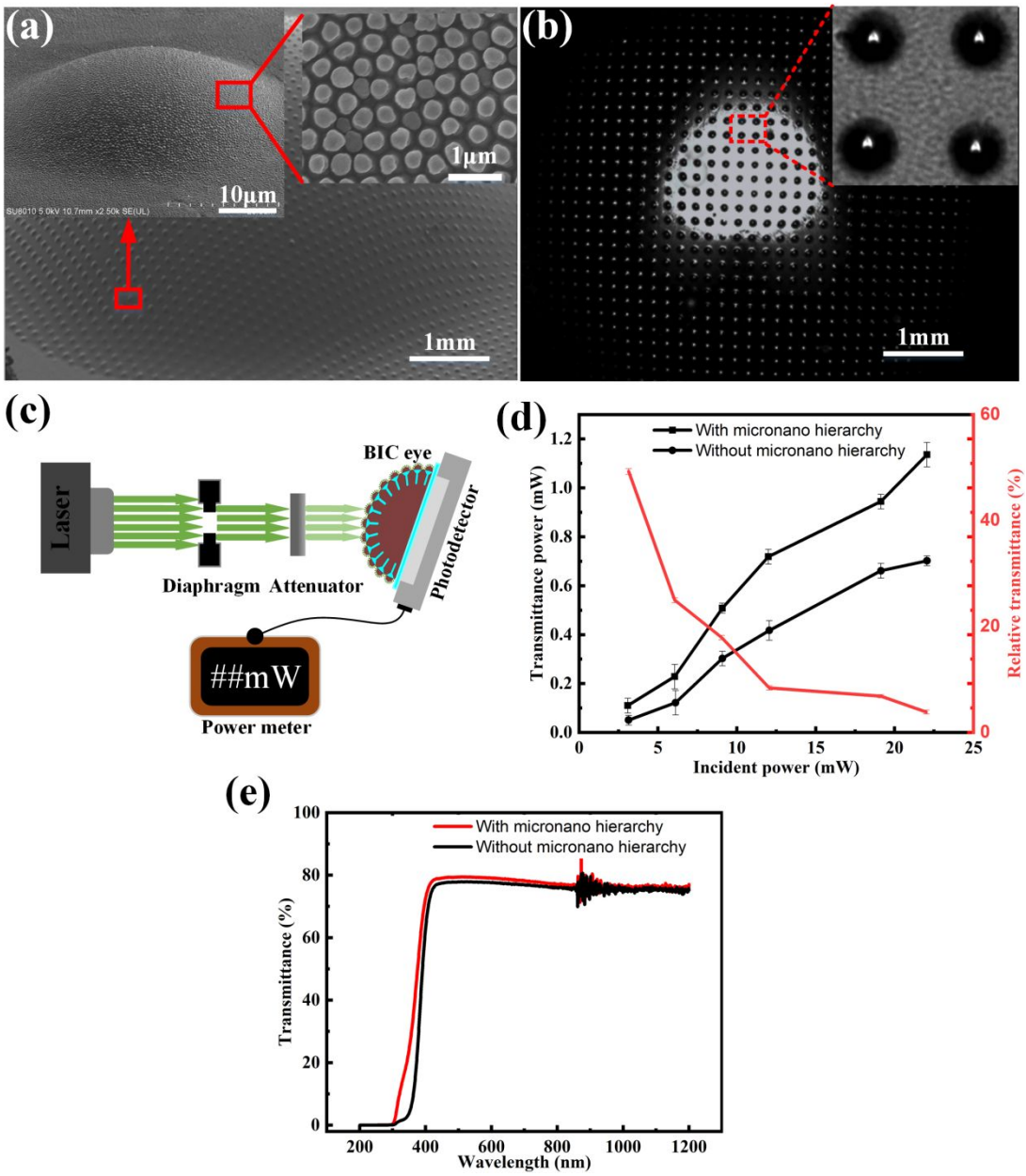

Figure 5. (a) SEM image of fabricated BIC eye, the inset are partial magnification. (b) Arrays of miniaturized "A" letters on the focal plane of the BIC illuminated by Tungsten lamp. (c) Schematic image of the optical characterization system. (d) The transmittance comparison of compound eye with and without micronano structures for different incident power. (e) The transmittance comparison of compound eye with and without micronano structures for wavelength range of 200-1200 nm.

Optical Performance of Fabricated Compound Eye

To experimentally characterize the large field of view (FOV) of the BIC eye, a measurement system consisting of a tungsten lamp, a 3D translation stage, an objective lens and a CCD camera was set up, as shown in Figure 6a. The light could be adjusted to irradiate on the BIC eye at different incident angles (θ). Figure 6b shows the CCD images of the laser patterns through microlens with planar distribution for θ equal to 0°, 10°, and 20°, respectively. It was observed that the light spot has nearly systematic distribution for normal incidence. For tilted incident light, the focus spot gradually distorted. When the titled angle increases to be 20°, the lateral extension becomes so evident that it affects the normal imaging of the microlens array. Thus, the FOV of planar microlens array was only ~ 40°. By comparison, for artificial compound eye with curved distribution, a clear image array was obtained when the incident angle was less than 60°. However, with an increase in incident angle, the area of the imaging array gradually decreases. When the angle exceeds 60°, the image array is very small. This result confirmed that the FOV of the artificial compound eye was larger than 120°. In theory, the FOV is determined from the height (h) and radius (R) of the macrobase. Thus, the FOV could be precisely tuned for various practical applications by controlling h and R. The theoretical FOV can be calculated by:[22]

$$\mathrm{FOV} = 2\arcsin^{2Rh/R^2 + h^2} \quad (4)$$

With h=2 mm and R=5 mm, the FOV is calculated to be 154.6°. The theoretical FOV

was ~180°, whereas the measured FOV was ~140°. The difference between the experimental and theoretical results may be attributed to the inherent planar photodetector. On the other hand, the hierarchical structures affect the light transmittance to some extent while suppressing the surface reflection.

To quantify the distortion rate of the artificial compound eye, the intensity distributions along the x and y axes for normally incident light are extracted from the microscope images, as shown in Figure 6c. The cross-sectional intensity distributions of a single focal spot along the x and y axes for θ equal to 0 are roughly identical, indicating that the BIC eye exhibits a good focusing property. Figure 6d shows the intensity of the focal spots measured from four symmetrical positions and they are demonstrated to have a high uniformity. In addition, for θ = 0°, 30°, and 60°, the intensity distribution of a single focal spot is characterized, and the x- and y-direction intensity distributions are compared, as shown in Figures 6e and 6f. The FWHM intensities are 1.95 μm (x axis) and 1.97 μm(y axis), respectively. It is possible that the small fluctuations in spot size along the x or y axis are caused by non-normal incidence of the laser. Hence, the FWHM could be considered as a constant, independent of the incident angle of the laser. This result demonstrates that the BIC eye with a hierarchical macro-/micro-/nano- structure has a wide FOV without imaging distortion.

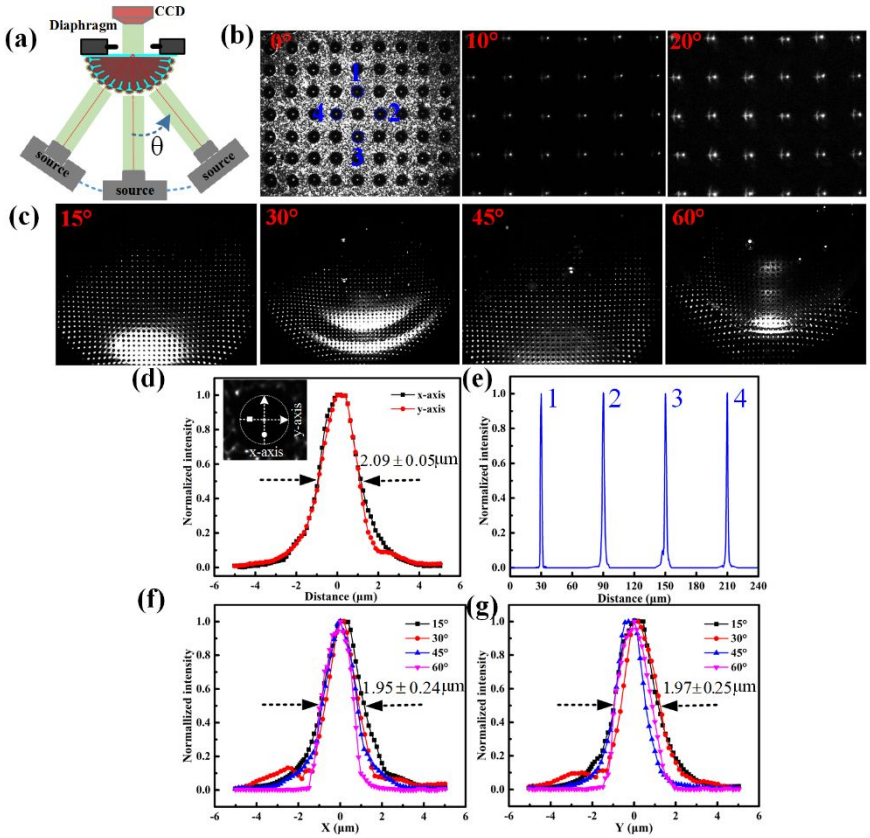

Figure 6. (a) Schematic image of the optical characterization system. (b-c) Output patterns of the planar microlens array and BIC eye irradiated by Tungsten lamp. (b) Planar microlens array irradiated at incident angles of 0°, 10°, and 20°, respectively. (c) Curved artificial compound eye irradiated at incident angels of 15°, 30°, 45°, and 60°, respectively. (d) Comparison of intensity distribution along x and y axes for normally incident light. Inset is a microscope image of a single focal spot. (e) Intensity of the focal spots from four symmetrical positions that demonstrate high uniformity. (f,g) Comparison of x- and y-direction normalized intensity distributions under incident angles of 15°, 30°, 45°, 60°, respectively.

FOV is an important property for artificial compound eye in practical application. According to equation (4), the FOV of fabricated structures could be adjusted by tuning the height and radius of the spherical base, as shown in Figure 7a.

Therefore, the FOV is a combined effect of both *R* and *h*. In the experiment, the height of base was tuned by adjusting *h*, while the *R* of spherical base was kept constant of 2.5 mm. Through tuning the base height, controllability of FOV was realized, as shown in Figure 7b. The side and top views of fabricated artificial compound eye are shown in insets of Figure 7b. The corresponding FOV are shown in Figure S2. In the experiment, the FOV of artificial compound eye could be ~140°. By addition of self-written waveguide to avoid optical crosstalk between microlens, improved FOV and imaging performance will be expected. The tunable FOV indicates various potential applications of fabricated hierarchical compound eye.

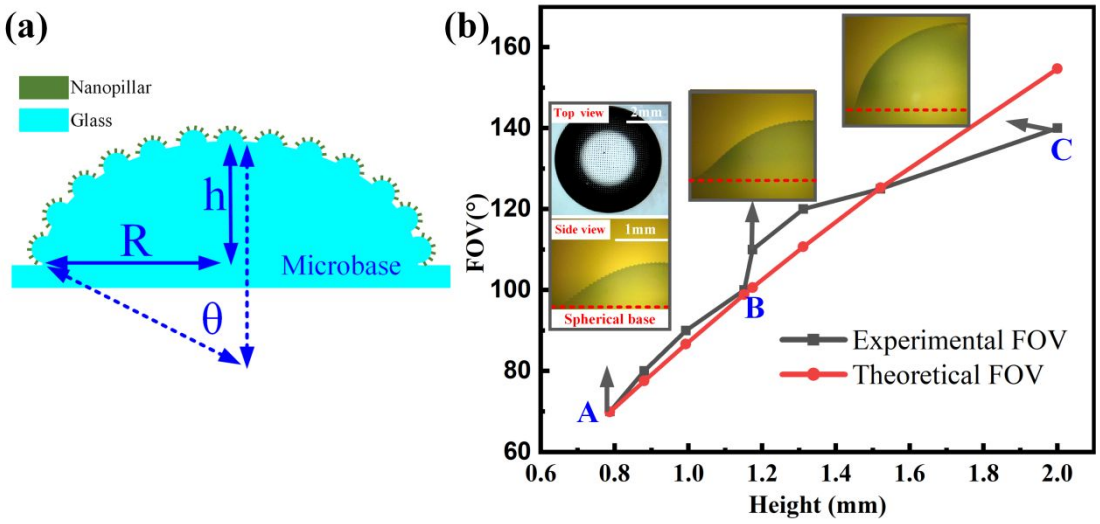

Figure 7. (a) Theoretical calculation of FOV of the artificial compound eye. (b) The tunable FOV of artificial compound eye was realized by adjusting the base height. The red and black curve show the theoretical and experimental relationship between the base height (*h*) and the FOV when the radius is kept constant of 2.5 mm. The insets show the side and top view of the fabricated artificial compound eye with different base height.

CONCLUSION

This paper has presented a manufacturing method that integrates nano-imprinting, picosecond laser swelling and air-assisted deformation for fabrication of macro-/micro-/nano- hierarchical compound eyes. The bioinspired compound (BIC) eyes with controllable size, high consistency, and low distortion made by this method show excellent morphology features and good optical performance. The tertiary (macro/micro/nano) structures endow a BIC eye excellent surface wettability with a contact angle (CA) of 152°, good light absorption rate of > 75% over the wavelength range of 400 to 800 nm, high quality imaging property, excellent weak light detection capability, and a wide field-of-view of 120° without distortion. These multifunctional properties enable the multi-scale compound eye to retain their superior optical performance in a wide range of real-time environmental conditions. The reported work should provide a beneficial direction for the widespread applications of the multi-scale compound eye such as wide-angle communication antenna, integrated optical circuits.

■ ASSOCIATED CONTENT

Supporting Information

Structures with controllable morphology were obtained by adjusting both the film thickness and pressure difference. The Dependence of curvature radius on film thickness of PDMS and press difference (Figure S1). Controllable FOV was achieved by adjusting the height of fabricated artificial compound eyes. The imaging of artificial compound eye with different light incident angles (Figure S2).

■ AUTHOR INFORMATION

Corresponding Author

* E-mail: wenjunwang@xjtu.edu.cn.

■ ACKNOWLEDGEMENTS

This work was supported by the National Key Research and Development Program of China (grant no. 2017YFB1104602).

■ REFERENCES

(1) Fitzgerald, R. J. Artificial Compound Eyes. *Phys. Today* **2006,** *59*, 21-21.

(2) Jeong, K. H.; Kim, J.; Lee, L. P. Biologically Inspired Artificial Compound Eyes. *Sci.* **2006,** *312*, 557-561.

(3) Ko, D. H.; Tumbleston, J. R.; Henderson, K. J.; Euliss, L. E.; DeSimone, J. M.; Lopez, R.; Samulski, E. T. Biomimetic Microlens Array with Antireflective "Moth-Eye" Surface. *Soft Matter* **2011,** *7*, 6404-6407.

(4) Peng, L. F.; Zhang, C. P.; Wu, H.; Yi, P. Y.; Lai, X. M.; Ni, J. Continuous Fabrication of Multiscale Compound Eyes Arrays With Antireflection and Hydrophobic Properties. *IEEE T. Nanotechnol.* **2016,** *15*, 971-976.

(5) Li J., Wang W., Mei X., Pan A., Sun X., Liu B.; Cui J., Artificial Compound Eyes Prepared by a Combination of Air-Assisted Deformation, Modified Laser Swelling, and Controlled Crystal Growth. *ACS Nano* **2019**,13(1), 114-124.

(6) Shao, J.; Ding, Y.; Wang, W.; Mei, X.; Zhai, H.; Tian, H. Generation of Fully-covering Hierarchical Micro-/nano- Structures by Nanoimprinting and Modified Laser Swelling. *Small*, **2014**, 10(13), 2595-2601.

(7) Wei, W. R.; Tsai, M. L.; Ho, S. T.; Tai, S. H.; Ho, C. R.; Tsai, S. H.; Liu, C. W.; Chung, R. J.; He, J. H. Above-11%-efficiency Organic-inorganic Hybrid Solar Cells with Omnidirectional Harvesting Characteristics by Employing Hierarchical Photon-trapping Structures. *Nano Lett.* **2013,** *13* (8), 3658-3663.

(8) Wu, D.; Wu, S. Z.; Niu, L. G.; Chen, Q. D.; Wang, R.; Song, J. F.; Fang, H. H.; Sun, H. B., High Numerical Aperture Microlens Arrays of Close Packing. *Appl. Phys. Lett.* **2010,** *97*, 031109.

(9) Daniela, R.; Jacques, D. E.; Uwe, D. Z.; Andreas, T. U. Laser Lithographic Fabrication and Characterization of a Spherical Artificial Compound Eye. *Opt. Express* **2007,** *15*, 3067-3077.

(10) Bian, H.; Wei, Y.; Yang, Q.; Chen, F.; Zhang, F.; Du, G.; Yong, J.; Hou, X. Direct Fabrication of Compound-Eye Microlens Array on Curved Surfaces by a Facile Femtosecond Laser Enhanced Wet Etching Process. *Appl. Phys. Lett.* **2016,** *109* (22), 221109.

(11) Xu, M.; He, R.; Sun, S.; Aldana, J. R. V. d.; Chen, F. Femtosecond Laser Micromachined Optical Waveguides in LiTaO3crystal. *Phys. Status Solidi-R.* **2013,** *7* (11), 1014-1017.

(12) Yong, J.; Chen, F.; Yang, Q.; Zhang, D.; Bian, H.; Du, G.; Si, J.; Meng, X.; Hou, X. Controllable Adhesive Superhydrophobic Surfaces Based on PDMS Microwell Arrays. *Langmuir* **2013,** *29* (10), 3274-3279.

(13) Shao, J.; Ding, Y.; Zhai, H.; Hu, BF.; Li, X.; Tian, H. Fabrication of Large Curvature Microlens

Array Using Confined Laser Swelling Method. *Opt. Lett.* **2013,** *38*, 3044-3046.

(14) Li, J.; Wang, W.; Mei, X.; Sun, X.; Pan, A. The Formation of Convex Microstructures by Laser Irradiation of Dual-layer Polymethylmethacrylate (PMMA). *Opt. Laser Technol.* **2018,** *106*, 461-468.

(15) Sun, Y. L.; Dong, W. F.; Niu, L. G.; Jiang, T.; Liu, D. X.; Zhang, L.; Wang, Y. S.; Chen, Q. D.; Kim, D. P.; Sun, H. B. Protein-Based Soft Micro-Optics Fabricated by Femtosecond Laser Direct Writing. *Light-Sci. Appl.* **2014,** *3*, e129.

(16) Meunier, T.; Villafranca, A. B.; Bhardwaj, R.; Weck, A. Fabrication of Microlens Arrays in Polycarbonate with Nanojoule Energy Femtosecond Laser Pulses. *Opt. Lett.* **2012,** *37* (20), 4266-4268.

(17) He, Q.; Liu, J.; Yang, B.; Dong, Y. Z.; Yang, C. S. Fabrication and Characterization of Biologically Inspired Curved-Surface Artificial Compound Eyes. *J. Microelectromech. S.* **2013,** *22*, 4-6.

(18) Li, Z.; Xiao, J. Mechanics and Optics of Stretchable Elastomeric Microlens Array for Artificial Compound Eye Camera. *J. Appl. Phys.* **2015,** *117* (1), 014904.

(19) Serra, F.; Gharbi, M. A.; Luo, Y.; Liu, I. B.; Bade, N. D.; Kamien, R. D.; Yang, S.; Stebe, K. J. Curvature-Driven, One-Step Assembly of Reconfigurable Smectic Liquid Crystal "Compound Eye" Lenses. *Adv. Opt. Mater.* **2015,** *3* (9), 1287-1292.

(20) Chan, E. P.; Crosby, A. J. Fabricating Microlens Arrays by Surface Wrinkling. *Adv. Mater.* **2006,** *18* (24), 3238-3242.

(21) Koo, W. H.; Jeong, S. M.; Araoka, F.; Ishikawa, K.; Nishimura, S.; Toyooka, T.; Takezoe, H. Light Extraction from Organic Light-Emitting Diodes Enhanced by Spontaneously Formed Buckles.

Nat. Photonics **2010,** *4* (4), 222-226.

(22) Wu, D.; Wang, J. N.; Niu, L. G.; Zhang, X. L.; Wu, S. Z.; Chen, Q. D.; Lee, L. P.; Sun, H. B. Bioinspired Fabrication of High-Quality 3D Artificial Compound Eyes by Voxel-Modulation Femtosecond Laser Writing for Distortion-Free Wide-Field-of-View Imaging. *Adv. Opt. Mater.* **2014,** *2*, 751-758.

(23) Deng, Z. F.; Chen, F.; Yang, Q.; Bian, H.; Du, G. Q.; Yong, J. L.; Shan, C.; Hou, X., Dragonfly-Eye-Inspired Artificial Compound Ees with Sphisticated Imaging. *Adv. Funct. Mater.* **2016,** *26*, 1995-2001.

(24) Wang, T.; Yu, W.; Li, C.; Zhang, H.; Xu, Z.; Lu, Z.; Sun, Q. Biomimetic Compound Eye with a High Numerical Aperture and Anti-Reflective Nanostructures on Curved Surfaces. *Opt. Lett.* **2012,** *37*, 2397-2399.

(25) Raut, H. K.; Dinachali, S. S.; Loke, Y. C.; Ganesan, R.; Ansah-Antwi, K. K.; Góra, A. Multiscale Ommatidial Arrays with Broadband and Omnidirectional Antireflection and Antifogging Properties by Sacrificial Layer Mediated Nanoimprinting. *ACS Nano* **2015**, 9, 1305-1314.

(26) Kuo, W. K.; Kuo, G. F.; Lin, S. Y.; Yu, H. H., Fabrication and Characterization of Artificial Miniaturized Insect Compound Eyes for Imaging. *Bioinspir. Biomim.* **2015,** *10*, 056010.

(27) Duparre, J. W.; Wippermann, F. C. Micro-optical Artificial Compound Eyes. *Bioinspir Biomim* **2006,** *1* (1), R1-16.

(28) Xu, H.; Lu, N.; Shi, G.; Qi, D.; Yang, B.; Li, H.; Xu, W.; Chi, L. Biomimetic Antireflective Hierarchical Arrays. *Langmuir* **2011,** *27*, 4963-4967.

(29) Wu, F.; Shi, G.; Xu, H.; Liu, L.; Wang, Y.; Qi, D.; Lu, N. Fabrication of Antireflective Compound Eyes by Imprinting. *ACS Appl. Mater. Inter.* **2013,** *5*, 12799-12803.

(30) Liu, H.; Huang, Y.; Jiang, H. Artificial Eye for Scotopic Vision with Bioinspired All-Optical Photosensitivity Enhancer. *P. Natl. Acad. Sci. USA* **2016,** *113*, 3982-3985.

(31) Wu, F.; Shi, G.; Xu, H.; Liu, L.; Wang, Y.; Qi, D. Fabrication of Antireflective Compound Eyes by Imprinting. *ACS Appl. Mater. Inter.*, **2013**, 5(24), 12799-12803.

(32) Beinhorn, F.; Ihlemann, J.; Luther, K.; & Troe, J. Micro-lens Arrays Generated by UV Laser Irradiation of Doped PMMA. *Appl. Phys. A-matter* **1999**, 68(6), 709-713.

(33) Himmelbauer, M.; Arenholz, E.; Bäuerle, D.; & Schilcher, K. UV-laser-induced Surface Topology Changes in Polyimide. *Appl. Phys. A* **1996**, 63(4), 337-339.

(34) Dong, S. K.; Lee, H. S.; Lee, B. K.; Sang, S. Y.; Tai, H. K.; & Lee, S. S. Replications and Analysis of Microlens Array Fabricated by a Modified Liga Process. *Polym. Eng. Sci.* **2010**, 46(4), 416-425.

(35) Malyshev, A. Y.; Agareva, N. A.; Bityurin, N. M.; Mal'shakova O. A. The Formation of Convex Microstructures on the Surface of Polymeric Materials under Laser Irradiation. *J. Opt. Technol.* **2007**, 74(9), 641-646.

(36) Ahsan, M.S.; Dewanda, F.; Lee, M.S.; Sekita, H.; Sumiyoshi, T. Formation of Superhydrophobic Soda-lime Glass Surface using Femtosecond Laser Pulses. *Appl. Surf. Sci.* **2013**, 265, 784–789.

Graphic for manuscript

(For Table of Contents Only)